Catchment-scale mapping of surface grain size in gravel bed rivers using airborne digital imagery

Patrice E. Carbonneau and Stuart N. Lane
Department of Geography, University of Durham, Durham, UK

Normand E. Bergeron
Institut National de la Recherche Scientifique, Centre Eau, Terre et Environnement, Sainte-Foy, Quebec, Canada

Received 9 October 2003; revised 23 March 2004; accepted 27 April 2004; published 22 July 2004.

[1] This study develops and assesses two methods for estimating median surface grain sizes using digital image processing from centimeter-resolution airborne imagery. Digital images with ground resolutions of 3 cm and 10 cm were combined with field calibration measurements to establish predictive relationships for grain size as a function of both local image texture and local image semivariance. Independently acquired grain size data were then used to assess the algorithm performance. Results showed that for the 3 cm imagery both local image semivariance and texture are highly sensitive to median grain size, with semivariance being a better predictor than image texture. However, in the case of 10 cm imagery, sensitivity of image semivariance and texture to grain size was poor, and this scale of imagery was found to be unsuitable for grain size estimation. This study therefore demonstrates that local image properties in very high resolution digital imagery allow for automated grain size measurement using image processing and remote sensing methods. *INDEX TERMS:* 1824 Hydrology: Geomorphology (1625); 1899 Hydrology: General or miscellaneous; 1815 Hydrology: Erosion and sedimentation; *KEYWORDS:* fluvial grain size measurement, airborne remote sensing, digital image processing, image semivariance, image texture

Citation: Carbonneau, P. E., S. N. Lane, and N. E. Bergeron (2004), Catchment-scale mapping of surface grain size in gravel bed rivers using airborne digital imagery, *Water Resour. Res.*, *40*, W07202, doi:10.1029/2003WR002759.

1. Introduction

[2] Grain size measurements of fluvial gravels are a fundamental descriptor for many fields of geomorphological research, including sediment transport [e.g., *Middleton and Southard*, 1984; *Wiberg and Smith*, 1987] and the study of flow resistance and the prediction of flow velocities in open channel flow [e.g., *Bray*, 1982; *Clifford et al.*, 1992]. Furthermore, grain size has also been demonstrated to be an important variable for the habitat preferences of salmonids [e.g., *Rimmer et al.*, 1983; *Cunjak*, 1988; *Heggenes*, 1996]. Methods for the field measurements of the grain size distributions of fluvial sediment are well established and are the subject of many studies [*Wolman*, 1954; *Hey and Thorne*, 1983; *Church et al.*, 1987; *Rice and Church*, 1996; *Bunte and Abt*, 2001]. Generally, these methods are labor intensive and require a significant amount of fieldwork to implement. Consequently, the time needed to acquire grain size measurements may limit the size of the area that can be sampled.

[3] However, there has been growing interest in the development of methods which could potentially reduce the field effort associated with grain size data collection and so increase the area that may be sampled. These methods typically rely on photographs of the bed. Also called photosieving, they involve taking plan view images of gravels either in exposed areas [*Adams*, 1979; *Ibbeken and Schleyer*, 1986; *Butler et al.*, 2001a] or shallow submerged areas [*Whitman et al.*, 2003]. Generally, images of the riverbed are collected from standing position with some form of scale information in each image. This yields images that cover up to $\sim$1 m^2 (e.g., 0.4 m^2 [*Bunte and Abt*, 2001]). These images are then analyzed either using manual measurements [e.g., *Adams*, 1979] or using automated image segmentation and measurement [*Butler et al.*, 2001a]. The main advantage of photosieving lies in the fact that actual measurement of the clasts does not take place in the field, which saves field effort. However, photosieving has three main disadvantages. First, the method is limited to measurement of the visible surface of gravels. Therefore photosieving is not applicable in cases where subsurface grain sizes are required. Second, the minimal clast size that can be analyzed is typically in the gravel range, for example, *Ibbeken and Schleyer* [1986] only considered particles coarser than 20 mm, and *Butler et al.* [2001a] followed the recommendations of *Wolman* [1954], designed for manual grain size measurements, and set the lower threshold of measurable size to 8 mm. These thresholds are directly related to image scale. Provided that sufficient image texture is present, higher-resolution imagery should allow for the detection of sand and silt particles. However, given current imaging technology, the detection of individual sand grains would require images with extremely low spatial coverage, of the order of a few square centimeters. This is clearly not practical for reach of river-scale studies, and thus photosieving is not applicable to sands, silts, and clays and is more suitable to gravely environments. The

0043-1397/04/2003WR002759$09.00

third difficulty with photosieving methods involves the use of two-dimensional imagery, which introduces a systematic underestimation of clast dimension and requires correction [*Adams*, 1979]. This bias has two causes. The first is the approximation of the actual clast dimensions in three-dimensional space from their projection in a two-dimensional image. Second is that the hiding effect of neighboring, overlapping, and interlocking (i.e., armored) clasts will cause additional bias. *Ibbeken and Schleyer* [1986] have found that while photosieving does cause a bias, this bias is acceptably small and the correction may usually be neglected. *Adams* [1979] found a significant bias and used an appropriate correction factor. However, *Church et al.* [1987] note that the magnitude of this correction factor will depend on the degree of imbrication and the angle of the clasts within the bed fabric. Therefore generalized correction factors are difficult to justify.

[4] The computer automation of photosieving techniques could allow for a significant increase in the volume of grain size information that is collected. However, even if automated methods were applied to process 0.4 m^2 images, 1000 images would be required to cover 400 m^2. Such techniques are therefore limited to small river reaches and are impractical when grain size information over very large scales (>10 km) is of interest. For example, *Rice and Church* [1998] used grain size data sampled at the river scale to show that downstream fining is not continuous along a given river. This allowed for the development of the concept of the sedimentary link. Furthermore, *Fausch et al.* [2002] propose that fluvial habitat modeling of aquatic species must be extended to the scale of the entire river. Given that grain size distribution is a fundamental parameter of aquatic habitat [*Guay et al.*, 2000], catchment-scale grain estimations will be necessary. Since both field measurements and photosieving are not easily applicable at the river scale, there is a need for alternative methods.

[5] Airborne multispectral remote sensing techniques have already been successfully applied to large-scale geomorphological work in fluvial environments [*Winterbottom and Gilvear*, 1997; *Wright et al.*, 2000; *Zhang*, 2000; *Legleiter et al.*, 2002]. These authors demonstrated that it is possible to classify morphological units in fluvial environments such as pools, riffles, and rapids from multispectral imagery with resolutions ranging from 0.25 to 3 m. Furthermore, an empirical method of automated grain size measurement using a combination of centimeter-resolution airborne digital color imagery and close range millimeter resolution imagery has been proposed by *Verdú et al* [2003]. These authors used one-dimensional semivariance measurements combined with data acquired using close range imagery to determine grain size measurements from high-resolution airborne digital imagery. They report an R^2 value of 0.86 between predicted and observed values for grain sizes.

[6] The work presented here is part of a larger research project, GEOSALAR, which aims to apply geomatics and remote sensing techniques to river-scale mapping of the physical habitat of Atlantic salmon (*Salmo salar L.*). The specific objective of this work is to obtain an automated method of grain size estimation capable of yielding reliable values for the median diameter (D_{50}) of dry exposed surface gravels, with a spatial resolution of the order of 1 m. This study first considers both image texture and two-dimensional semivariance as theoretical bases for the estimation of grain sizes from airborne imagery. These tools are tested on two sets of digital imagery with ground resolutions of 3 and 10 cm. Ground truth grain size data were correlated to local image properties in order to establish predictive relationships. Subsequently, independent validation of the predictive relationships was carried out with manually collected field data. The validation results show that the observed correlation between local image texture and grain size is less reliable than the correlation relationship between grain size and local semivariance. Therefore local image semivariance was used to develop a new method for fully automated grain size measurement from high-resolution digital airborne imagery.

2. Mapping Grain Size From Airborne Imagery: Theoretical Considerations

[7] This section presents the currently known image processing theory and established methods that could allow for the development of automated grain size mapping. In order to develop automated grain size mapping, quantitative image properties which can be used to predict the size of gravels in an image must be found. These properties can then be used to predict grain sizes in either a physical modeling approach or an empirical modeling approach.

[8] Physical modeling involves the use of known physical properties of the gravel patches under a given illumination to predict the radiometric and reflective characteristics of the gravels as a function of their grain size. Such approaches have been applied with success in the field of canopy reflectance modeling [*Baret et al.*, 1994; *Borel and Gerstl*, 1994]. In the case of fluvial gravels, the main image characteristic is the presence of light-dark contact zones created by gravels and their shadow. It is reasonable to assume that these light-dark contact zones will be affected by grain size since larger particles will have larger light areas and will also produce larger shadows. Therefore predicting the radiometric and reflective characteristics of gravels would require physical models for the reflection and dispersion of light and the statistical spatial distribution of shaded areas as a function of surface roughness, gravel lithology, and illumination. While some progress has been made in the field of modeling the roughness of gravels [*Robert*, 1991; *Bergeron*, 1998; *Butler et al.*, 2001b], the modeling of the spatial distributions of shaded areas and the prediction of gravel image texture as a function of lighting conditions and particle size remains an extremely complex and difficult problem. This difficulty is reflected in the absence of published work describing methods of grain size estimation based on the physical prediction of their image texture.

[9] The empirical approach is a black box method that seeks to establish a statistical relationship between local image properties and ground truth data. This approach is conceptually simpler and, if properly applied, could allow for a characterization of the complex image textures associated with fluvial gravels. However, appropriate image properties that are highly sensitive to image texture must be identified. Furthermore, calibration data are required in order to establish an empirical predictive relationship be-

tween an image property and grain size. Examination of the available literature reveals two image properties that could potentially be used for grain size mapping: image texture and semivariance.

[10] Image texture, as defined by the cooccurrence matrix, was among the first local image properties to be developed capable of segmenting image areas that appear visually distinct to a human observer [*Haralick et al.*, 1973; *Haralick*, 1979; *Conners et al.*, 1984]. It is therefore reasonable to hypothesize that image texture may allow for grain size determination since patches of different grain sizes appear distinct to a human observer provided image resolution is sufficient. Semivariance is also frequently employed in digital image processing [*Wulder and Boots*, 1998]. For example, *Miranda and Carr* [1994] have shown that semivariance can distinguish between different species of vegetation when applied to spaceborne imaging radar-B (SIR-B) imagery, and *Verdú et al.* [2003] have successfully used semivariance to predict grain sizes. Image semivariance and texture were therefore tested as possible image properties capable of deriving grain size from airborne digital imagery.

[11] Image texture is defined as an attribute representing the spatial arrangement of the gray levels of the pixels in a region [*Institute of Electrical and Electronics Engineers* (*IEEE*), 1990]. Texture-based analysis operates by transforming a raw image into a textural image, where regional texture information is represented as gray levels. Image texture is evaluated with the cooccurrence matrix. The cooccurrence matrix is constructed by comparing all image pixels separated by a distance D at direction $\vec{d}$. The i, jth element of the cooccurrence matrix $\mathbf{P}$ for an image is the number of times that gray levels i and j occur in two pixels separated by distance D and direction $\vec{d}$ divided by the total number of pixel pairs [*Castleman*, 1996]. Therefore cooccurrence can quantify how many pixels of similar gray levels are neighbors. The cooccurrence matrix is of size (L, L), where L is the number of gray levels in the image (256 for 8 bit gray scale images). However, calculation of a 256 $\times$ 256 cooccurrence matrix remains computationally demanding even with current desktop computers. To make computation times manageable, images are typically resampled to 8, 16, or 32 gray levels. Once the cooccurrence matrix is calculated, textural features may be derived to reduce the information in the cooccurrence matrix to a single value [*Haralick et al.*, 1973; *Conners et al.*, 1984; *Castleman*, 1996]. Among these textural inertia is of particular interest in this case. Textural inertia is a dimensionless parameter defined as [*Conners et al.*, 1984]

$$I = \sum_{i=0}^{L-1} \sum_{j=0}^{L-1} (i-j)^2 \mathbf{P}_{ij}, \tag{1}$$

where I is the textural inertia and i and j are the brightness levels in the cooccurrence matrix $\mathbf{P}$ of size (L, L). The form of equation (1) justifies its potential interest for the present application. The term $(i-j)^2$ has the effect of eliminating the contribution of diagonal terms in the cooccurrence matrix where $I = j$. Furthermore, the exponent in the term has the effect of exaggerating the contribution of values in the cooccurrence matrix where i greatly differs from j. Therefore textural inertia hides areas where equal brightness levels are in contact, and it highlights areas where different brightness levels are in contact. This should be well suited to images of gravel beds characterized by light-dark contact areas between uniform colored clasts and shaded zones.

[12] The second property under consideration is local semivariance. *Verdú et al.* [2003] used one-dimensional semivariance estimates originally developed for the analysis of one-dimensional data. However, one-dimensional semivariance is defined for one-dimensional, time series–type data. It is therefore not capable of processing data arranged in a raster format such as a digital image. It is therefore necessary to extend one-dimensional semivariance to two dimensions if the information content of digital images is to be fully exploited. Two-dimensional semivariance can be defined by the following [*Carbonneau et al.*, 2003]:

$$\gamma(p,q) = \frac{1}{2(N-|p|)(M-|q|)} \sum_{i=1+\frac{|p|-p}{2}}^{N-\frac{|p|+p}{2}} \cdot \sum_{j=1+\frac{|q|-q}{2}}^{M-\frac{|q|+q}{2}} [Z(i+p,\, j+q) - Z(i,\, j)]^2, \tag{2}$$

where p and q are the lags in the x and y directions, M and N are the dimensions of the surface in the x and y directions, and $Z(i, j)$ is the variable of interest, in this case brightness level, at point (i, j). The two-dimensional semivariogram is therefore a raster of values giving half the variance for every combination of lags p and q. Semivariance has units that are the square of the units of Z. For images, brightness values are dimensionless. Therefore image semivariance is dimensionless and will be referred to without units throughout this article.

[13] The semivariance recognizes that the variance in brightness levels between pixels separated by a certain distance will be a function of that distance. For the case of a raster image with a checkerboard pattern (i.e., alternating white and black pixels in a raster) the maximum semivariance will be reached for a lag of 1. If the checkerboard is made of alternating 2 pixel $\times$ 2 pixel areas, the maximum semivariance will be reached for a lag of 2. Hence there should be a relationship between the grain size of an image patch and the lag at which the maximum semivariance (the sill) is reached. However, this does not take into account the discretization effects encountered when sampling real continuous phenomena with discreet pixels of finite size. If the grains are smaller than the pixel size (also called pixel ground footprint), then one pixel will sample several grains and their associated shadow areas. Therefore the brightness level of the pixel will have a mixed spectral signature, and its brightness will be an averaged value. The semivariance sill for a raster of such pixels cannot be clearly related to the grain size. However, the semivariance value of the sill should be reduced due to the averaging effect of the sampling which reduces the difference between maximum and minimum brightness values. As particles in the image get coarser, there is an increased probability that pixels will cover more homogeneous zones of light or shadow. Therefore the pixel brightness values will more closely represent the actual continuous illumination variations of the surface and less averaging will occur. Thus the maximum difference between light and dark areas will be increased, and the

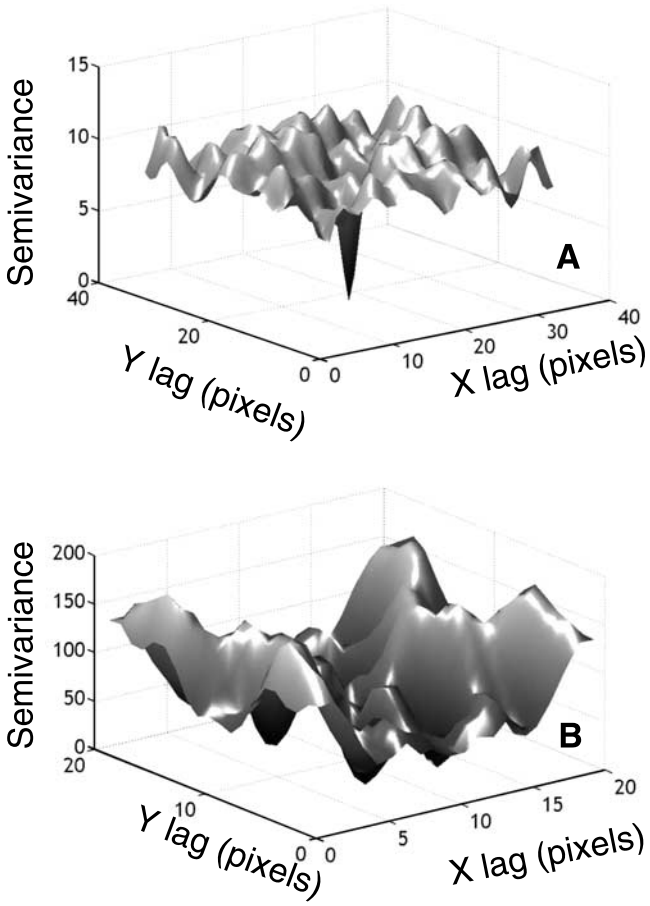

Figure 1. Examples of two-dimensional semivariograms illustrating both sill plane presence and absence. (a) Two-dimennsional semivariogram for a 33 × 33 pixel image. (b) Two-dimensional semivariogram for a 20 pixel × 20 pixel image.

semivariance sill value will also be of higher magnitude. It can therefore be hypothesized that grain size can be correlated with the sill value of local image semivariance. Figure 1 shows an example of two semivariograms and illustrates that the sill plane is sensitive to image size. The disappearance of the sill plane is symptomatic of nonstationarity caused by a trend in the image data [*Rossi et al.*, 1992]. Trends in image data are caused by objects of uniform color that are of comparable scale to the image. In such cases, the semivariogram will display a strong anisotropy which will reflect the orientation of the large object in the original image. The use of the semivariogram sill in image processing is therefore limited to cases where the objects in an image are much smaller than the total image dimensions.

3. Methods

3.1. Airborne Digital Imagery Acquisition

[14] Field work for the study was carried out on the 80 km long main branch of the Sainte-Marguerite River in Quebec, Canada. In August 2002, two helicopter surveys were carried out during the summer period of low flow. The XEOS™ system, developed by GENIVAR Inc., was used to obtain plan view digital imagery of the entire 80 km study area. The helicopter surveys were carried out at heights above the bed of 450 m and 155 m in order to obtain digital imagery with ground resolutions of 10 cm (1:1200 scale) and 3 cm (1:350 scale), respectively. Image format was 3008 pixels × 1960 pixels in the standard visible bands of red, green, and blue. Images were collected at 60% overlap to allow for photogrammetric work to be carried out in the future. Two days were required to complete the surveys yielding 1600 ten-centimeter-resolution images and 5600 three-centimeter-resolution images. Flights were carried out between 10:00 A.M. and 3:00 P.M. with weather conditions being generally cloudy and dry with infrequent sunny spells. Figure 2 shows examples of images for both available resolutions.

3.2. Photocontrol and Image Georeferencing

[15] Photocontrol points were collected with a Leica RTK GPS 500 system capable of centimeter-scale accuracy. Identifiable natural features such as logs and large clasts or man-made features such as roadside guard railings were used as targets for photocontrol. Additionally, ~600 artificial targets were placed along the river prior to the flight and were subsequently surveyed. This survey required ~3 weeks of field work to complete. Image georeferencing was undertaken using the georeferencing tool in ArcMap (ESRI

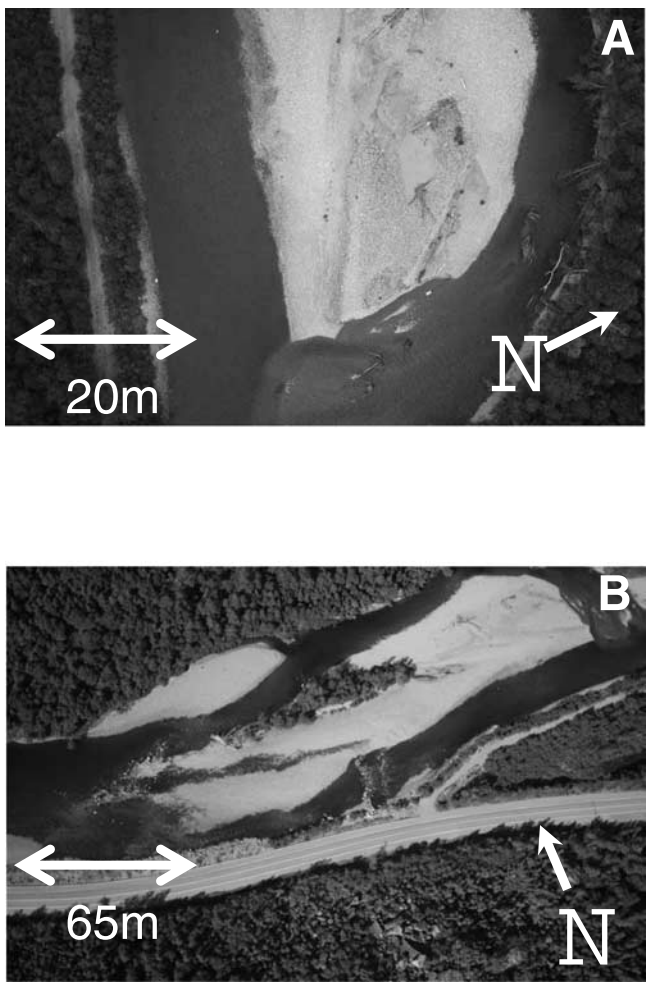

Figure 2. Examples of high-resolution airborne imagery from the Sainte-Marguerite River located at 48.38°N, 70.20°W: (a) 3 cm image; (b) 10 cm image.

Inc., Redlands, California). This tool allows the user to associate image points with their geographic coordinates. At least two points are required to perform the affine transformation that determines the orientation and scale of an image. When additional points are added, a least squares regression algorithm was applied to determine optimal georeferencing results. The quality of the georeferencing process was examined with the total RMS error output by ArcMap (ESRI Inc., Redlands, California). In this case, the mean RMS error for all 3 cm images was ±27.8 cm, and it was ±120 cm for 10 cm images.

3.3. Ground Truth Grain Size Data

[16] Grain sizes along the river range from coarse sand to boulder. In order to obtain a similar size range over a small reach, a midchannel bar covered by 10 images was selected as a pilot study site. This particular bar was selected because it presented the full range of grain sizes present along the river, thus allowing for reliable calibration of the methodology. Grain size calibration data were obtained with a close range photosieving technique selected to reduce the field time required to obtain ground truth data. Furthermore, by using plan view images as ground truth data, bias due to particle imbrication should be similar in both the ground truth images and the airborne images. Seventy plan view digital images were taken along the midchannel bar with a commercial digital camera. Image format was 1600 pixels × 1200 pixels. For each image, which covered about 1.2 m × 0.9 m (1.08 m^2), a ruler was placed in the top of the frame to establish scale. The center of the ruler was surveyed with the Leica RTK GPS 500 to establish the position of the close range images on the airborne photos. In anticipation of potential georeferencing errors, close range images were taken in the middle of uniform patches whose area exceeded 1 m^2.

[17] Grain sizes for these close range images were determined with a graphic user interface programmed in the MATLAB environment (The Mathworks Inc., Natik, Massachusetts). A 5 × 10 grid was first superimposed on the images. The user then manually identified with the mouse the *a* and *b* axis of clasts which were at the 50 grid intersections, and the program output the D_{50} for the image. A value of 0 mm was assigned to sand surfaces.

3.4. Image Classification

[18] Image processing was first applied to perform a classification of the dry bed areas using MATLAB (The Mathworks Inc., Natik, Massachusetts). Dry bed areas in the images were identified with histogram segmentation of the intensity band in hue-saturation-intensity (HSI) color format. HSI is an alternative color format to the widespread red-blue-green (RGB) format. Instead of representing color with three orthogonal components, as in the RGB format, the HSI format represents color in a spherical coordinate format where the hue and the saturation values are equivalent to the azimuthal and polar angles, respectively, and the intensity is equivalent to distance from the origin. In the intensity band, dry exposed gravels have a higher brightness value and are well suited to automated thresholding methods. In this case, Otsu's method [*Otsu*, 1979] was applied to isolate the dry exposed gravels from the rest of the image. This histogram-based method is designed to produce a segmentation threshold that minimizes the variance within the two resulting classes in the histogram. The performance of the classification algorithm was verified by selecting 10 images and manually tracing contours of the dry bed areas and comparing surface dimensions of manual and automated classification as a percentage. For dry bed areas the mean difference is 3.1%, and the standard deviation of the difference is 4.2%. Figure 3 presents a binary classification with dry bed areas in black.

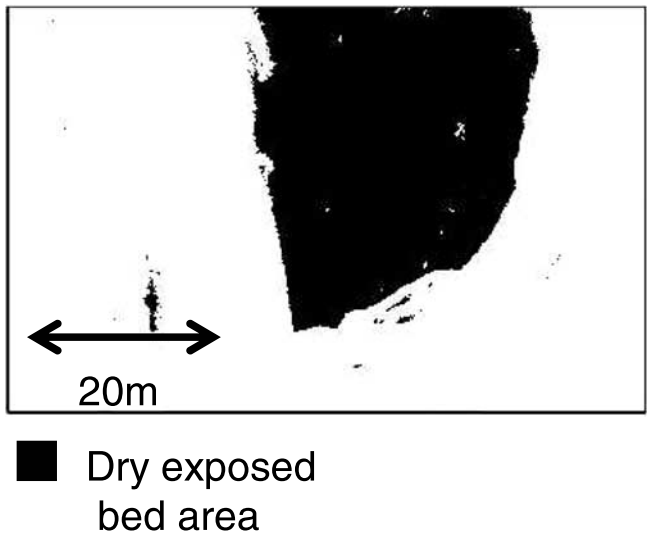

Figure 3. Binary image showing automatically detected dry bed areas in Figure 1a.

3.5. Image Corrections

[19] The classification results were used to correct the images before grain size estimation procedures. For each grain size estimation method discussed in section 2, local image texture correlation, and local two-dimensional semivariance correlation a different correction was applied, irrespective of image resolution. Image texture was found to be sensitive to illumination changes in the imagery that can be caused by variations in daylight or camera exposure times. Therefore the brightness of the images was corrected to compensate for illumination changes during the air survey. It was found that conventional histogram equalization or histogram stretches saturated the brightness levels in large areas and thus gave poor results. Therefore a simple histogram shift was applied to give dry gravel patches an equal mean brightness level of 150. Semivariance methods, which operate on the basis of differences in brightness levels, are insensitive to histogram shifts. However, semivariance methods would predictably be very sensitive in edge areas where the dark colored wetted perimeter pixels are in contact with lighter dry bed pixels. Therefore the classification results were used to reset the brightness levels of all pixels in the wetted and vegetated areas (the "not" dry area in the Boolean logic sense) of the image to the mean dry bed pixel value. This resulted in a reduced contrast along the edges of the dry bed area.

3.6. Mapping Local Image Properties: The Sampling Window Method

[20] The image properties described in section 2 are typically calculated for entire images. However, if the entire image is reduced to single semivariance sill plane or textural

inertia value, spatial location of texture and semivariance information are lost. It is therefore necessary to adopt a sampling window mapping approach. Instead of calculating texture and semivariance for the entire image, these properties are calculated for a small subsample of the image, the sampling window. By displacing the sampling window over the image it is possible to map local image properties and thus retain spatial information about the variation of local image properties. The resulting property map will hereafter be termed the property image. Thus the semivariogram or cooccurrence is calculated for each window of size (W, W) in the original (M, N) image. Semivariance is then reduced to a single value by taking the mean value of the sill plane, and cooccurrence is expressed by the inertia value. The resulting image has dimensions (M/W, N/W). Therefore, in the property image the i, jth pixel is the local property value in the region [i:$i + W - 1$; j:$j + W - 1$] of the original image. These property images can be used to test for correlation between local image properties and grain size in airborne digital imagery.

3.7. Optimal Window Size Selection

[21] The sampling window method requires the selection of a suitable window size. Since no theoretical guidelines exist for the optimal determination of window sizes, several window sizes were tested in order to assess the sensitivity of varying window sizes and to produce guidelines for optimal window size selection. The study objective of producing grain size maps with a spatial resolution of 1 m was used to obtain starting values of window size. This corresponds to 33 pixels $\times$ 33 pixels in the 3-cm-resolution imagery and 10 pixels $\times$ 10 pixels in the 10 cm imagery. The range of window sizes, selected to include these values, was therefore set to 5 $\times$ 5, 10 $\times$ 10, 20 $\times$ 20, 33 $\times$ 33, and 50 $\times$ 50. Property images for semivariance and texture were calculated for all window sizes and for both image resolutions. This yielded 20 distinct grain size data sets that will require calibration and validation.

3.8. Predictive Model Calibration

[22] Once the 20 property images were calculated, the values of semivariance or texture were extracted at the locations where ground truth data was available. The position of the ground truth grain size data was found by interpolating the property image to the same resolution as the original RGB image. A new false color image was then created by substituting the blue band with the property image. In order for this operation to work the property data must be rescaled, with a linear function, to the range [0 255]. This false color image was then automatically georeferenced by applying the same ground control point file as for the original RGB image. Thus the value of the false blue band, the property band, was read at the coordinates of the ground truth data and retransformed to the original property values with the scaling relationship. The ground truth b axis grain sizes were then plotted against the extracted local image properties for each given location. The relationships thus obtained, if any, could then be applied to estimate grain sizes in areas where no ground truth data was available.

3.9. Model Validation

[23] In order to validate the predictive relationships established between image properties and grain sizes, independent data was obtained (C. Davey, personal communication, 2003). This data set consists of 15 manual bulk sampling measurements of the b axis D_{50} of the dry bed armor layer. The D_{50} of the armor (i.e., surface) layer was selected because it corresponds to the visible portion of the bed material. Furthermore, since bulk sampling involves the removal and measurement of all the particle of the armor layer, irrespective of their size, this method removes any photosieving-type errors associated with the hiding effect of overlapping clasts and the minimal clast size restrictions. The data collection sites were scattered along a 10 km stretch of the Sainte-Marguerite River. Therefore each data point could be found on a single image, none of which have been used in the correlation model. Grain size maps were therefore calculated for these 15 images. Data point locations were provided with a precision estimated at ±1 m. Therefore predicted grain sizes for each validation point location were extracted from the grain size maps by taking the mean grain size calculated in a 1 m $\times$ 1 m window centered on the point location. Predicted grain sizes versus observed grain sizes were then plotted to establish model validity. Furthermore, the mean and standard deviation of the differences between predicted and observed points were calculated to obtain quality assessment. These results are expressed both as absolute values, in centimeters, and in normalized form, as a percentage of the local D_{50}.

4. Calibration and Validation Results

[24] Table 1 gives the results of the model calibration relationships according to the size of the window that was used (both in pixel units and in centimeters), the resolution of the images, and the image property that was applied. In Table 1 the NS entry signifies that semivariograms for a given window size did not have a sill plane and thus that the method is inapplicable.

[25] It was decided that only models where the majority of the variability was explained (i.e., with an $R^2 > 0.5$) would be studied further and validated. R^2 values in Table 1 range from 0.27 to 0.8. Acceptable levels of explanation are only found in the case of 3 cm imagery. In total, five models were validated. For the local image texture method, 20 $\times$ 20 windows, 33 $\times$ 33 windows, and 50 $\times$ 50 windows applications were validated. For the local semivariance method, only the 33 $\times$ 33 window and the 50 $\times$ 50 window were considered. Table 2 presents the results of the model validation carried out with the independent data. While the R^2 values indicate good linear relationships between observed and predicted data, slope values for the regressions show many cases where predicted values are underestimated. Furthermore, high bias values (intercepts) can be observed in most cases. However, in the case of the 33 $\times$ 33 window used with local semivariance, validation results are excellent. This model was therefore selected as the optimal method for this study. Figure 4 shows the regression plots for calibration and validation of this selected method. The error for the method was examined further with the mean and standard deviation of the differences between observed and predicted values. The mean difference was -0.28 cm with a standard deviation of 1.39 cm. If normalized by the overall D_{50}, this is a bias (systematic error) of -1.4% and a precision of ±15.4%. Once validated, the regression equation for the 33 $\times$ 33 sampling window applied to 3 cm

Table 1. Complete Results of Model Calibration Attempts[a]

Window Size, pixels	Pixel Size, cm	Actual Window Size, cm	Method	Slope	Intercept	R^2
5 × 5	3	15 × 15	T	35.26	27.78	0.33
10 × 10	3	30 × 30	T	47.00	18.54	0.44
20 × 20	**3**	**60 × 60**	**T**	**96.94**	**5.97**	**0.65**
33 × 33	**3**	**99 × 99**	**T**	**117.19**	**10.90**	**0.70**
50 × 50	**3**	**150 × 150**	**T**	**83.97**	**0.65**	**0.58**
5 × 5	3	15 × 15	SV	NS	NS	NS
10 × 10	3	30 × 30	SV	NS	NS	NS
20 × 20	3	60 × 60	SV	NS	NS	NS
33 × 33	**3**	**99 × 99**	**SV**	**0.34**	**10.12**	**0.80**
50 × 50	**3**	**150 × 150**	**SV**	**0.29**	**12.40**	**0.72**
5 × 5	10	50 × 50	T	82.97	31.36	0.39
10 × 10	10	100 × 100	T	78.19	−5.97	0.38
20 × 20	10	200 × 200	T	57.27	34.69	0.34
33 × 33	10	330 × 330	T	53.47	31.05	0.36
50 × 50	10	500 × 500	T	55.01	NS	0.39
5 × 5	10	50 × 50	SV	NS	NS	NS
10 × 10	10	100 × 100	SV	NS	NS	NS
20 × 20	10	200 × 200	SV	NS	NS	NS
33 × 33	10	330 × 330	SV	0.11	41.62	0.27
50 × 50	10	500 × 500	SV	0.11	39.96	0.27

[a]Bold entries indicate models that were studied further at the validation stage. T, texture; SV, semivariance; NS, "not suitable" data.

imagery can be used to predict grain sizes from semivariance property images (Figure 5).

5. Discussion

5.1. Guidelines for Successful Implementation of Grain Size Estimation Models

[26] On the basis of our results, six important parameters can be identified for successful implementation of grain size mapping: sampling window size (W), image resolution (i.e., pixel ground footprint) (R), scale of ground truth data (GT), scale of uniform gravel patches (GP), median particle size (D_{50}), and the minimum number of pixels required for a two-dimensional semivariogram to present a sill plane (SS). For grain size estimation to be successful the required relationship between these parameters can be inferred from our experimental results and expressed by the following equations:

$$W \geq \mathrm{SS}, \tag{3}$$

$$WR \leq \mathrm{GP}, \tag{4}$$

$$WR \approx \mathrm{GT}, \tag{5}$$

$$D_{50} \geq R. \tag{6}$$

[27] Equation (3) states that the sampling window must be of sufficient extent to ensure the presence of a sill plane in the semivariogram. As discussed in section 2, the absence of a sill plane renders the semivariance method unusable. In this particular case, if the sampling window is too small, it becomes possible for a few individual clasts to occupy a large part of the window. This will cause trend and lead to the disappearance of the sill plane. Table 1 and Figure 1 support this analysis by showing that for smaller window sizes, sill planes were not present.

[28] Equation (4) states that the ground footprint of the sampling window (i.e., the actual size of the window in real space), WR, should be smaller than the scale of uniform gravel patches in the study area. The semivariance and texture methods both implicitly assume that the area within the sampling window consists of a uniform gravel patch. Careful examination of the imagery used to calibrate the method (Figure 2a) and manual measurements of individual patches show that patch sizes range from 0.9 to 10 m^2. Therefore, in the cases where the ground footprint of the sampling window is greater than $\approx$1 m^2, the sampling window will frequently be straddling two or more uniform gravel patches. The effect of having multiple patches in a given sampling window was examined further by taking three image samples of 33 × 33 pixels at a resolution of 3 cm. The first consisted of uniform fine gravels. The area of the second sample was half covered by fine gravels with the other half covered by cobbles. Finally, the third consisted of uniform cobbles. The semivariograms and inertia values were then calculated and examined for these three samples. For the first sample, semivariance sill plane value was 284, and textural inertia was 1.2. For the second sample, semivariance sill plane value was 78, and textural inertia was 0.6. Finally, for the third sample, semivariance sill plane value was 42, and textural inertia was 0.08. The mean value of the sill plane for the mixed sample was therefore intermediate to those of the fine gravel and cobble samples. A similar result was obtained with the textural inertia values with the inertia of the mixed surface being between the inertias for fine gravels and cobbles. This

Table 2. Model Validation Results

Window Size	Method	Slope	Intercept	R^2
20 × 20	T	0.46	39.65	0.80
33 × 33	T	0.63	25.93	0.81
50 × 50	T	0.34	37.47	0.52
33 × 33	SV	1.03	0.57	0.96
50 × 50	SV	0.67	15.03	0.89

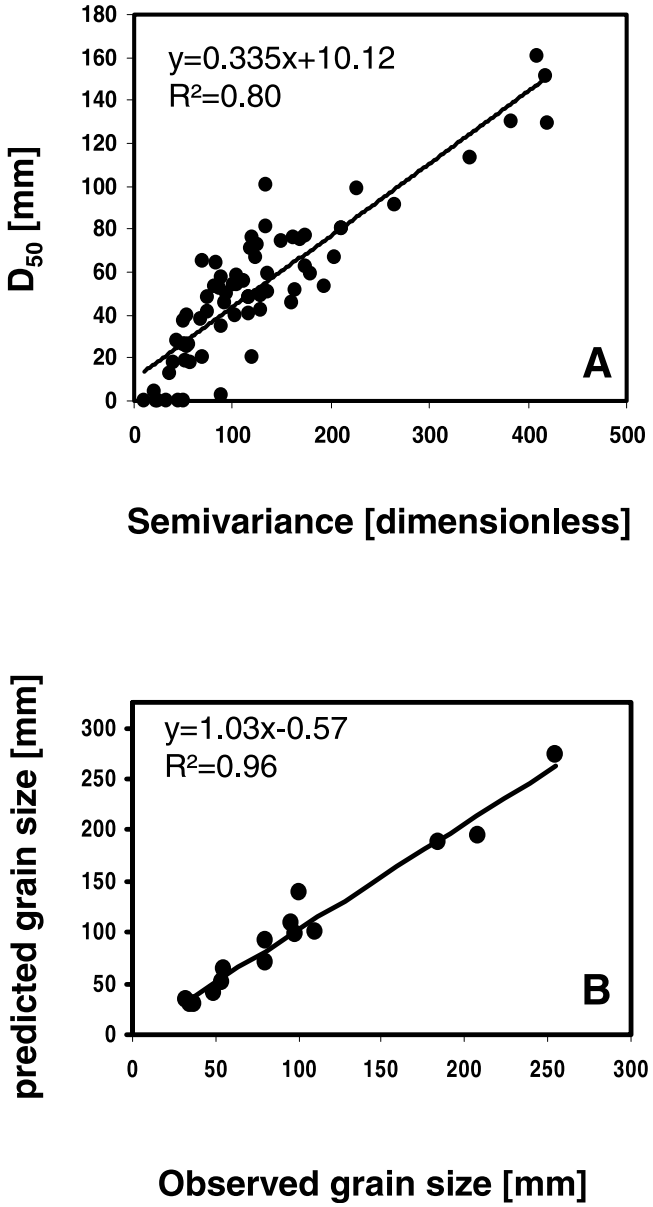

Figure 4. Regression plots showing the calibration and validation results of the semivariance method with a 33 pixel × 33 pixel window applied to 3 cm resolution imagery. (a) Calibration relationship of median diameter (D_{50}) versus semivariance. (b) Validation relationship of predicted versus observed median grain sizes (D_{50}) obtained from an independent data set.

means that if a sampling window straddles two (or more) patches, the local image property values will reflect an averaging of both patches. This is not a problem if the patch scale is greater than the sampling window. In such a case, contact areas between patches will yield a grain size gradient, but the central area of the patches will have semivariance and inertia values that reflect the grain size of the patch. However, if the patch scale is smaller than the sampling window, it will not be possible to interpret the inertia and semivariance sill values as being associated with a single grain size. Therefore, as window size increases, the statistical benefits gained by the larger sample size (i.e., larger window size) are offset by more than one grain size distribution appearing in the sample population, thus leading to a loss of model quality when window size is larger than the patch scale (equation (4)). This effect is clear in Tables 1 and 2, where a strong dependency on sampling window size can be seen. For both the textural and semivariance methods, validation quality degrades when comparing 33 × 33 and 50 × 50 windows. As indicated in Table 1, the ground footprint of 33 × 33 windows in 3 cm imagery is 99 cm × 99 cm. This corresponds almost exactly to the 1 m × 1 m scale of the ground truth imagery. In the case of the 50 × 50 windows, the ground footprint increases to 150 cm × 150 cm. Table 1 therefore shows that as the ground footprint departs from the 1 m^2 scale of the ground truth data, model quality degrades.

[29] A similar issue arises when considering the scale at which the ground truth data are collected. Equation (5) states that when establishing a correlation model between local image properties and ground truth grain size data, the area over which the ground truth grain sizes were measured should be comparable to the ground footprint sampling window size. If this is not the case and the sampling window is too large, when local image properties for the ground truth data area are evaluated, they will be affected by particles not measured in the ground truth data. This is likely to be one of the major factors contributing to the failure of grain size estimation in 10 cm imagery. Table 1 shows that in all attempts made with 10 cm imagery, results were poor. However, it is possible that if ground truth data were collected at the proper scale, useful grain size information could be collected from 10 cm airborne digital imagery.

[30] The final consideration is the image resolution with respect to particle size. Equation (6) states an idealized condition where the pixel size of the image is smaller than all particles in the image. Given that current airborne imaging technology is capable of centimeter-scale resolutions, the condition in equation (6) cannot be met for clays, silts, sands, and fine gravels. It is therefore necessary to

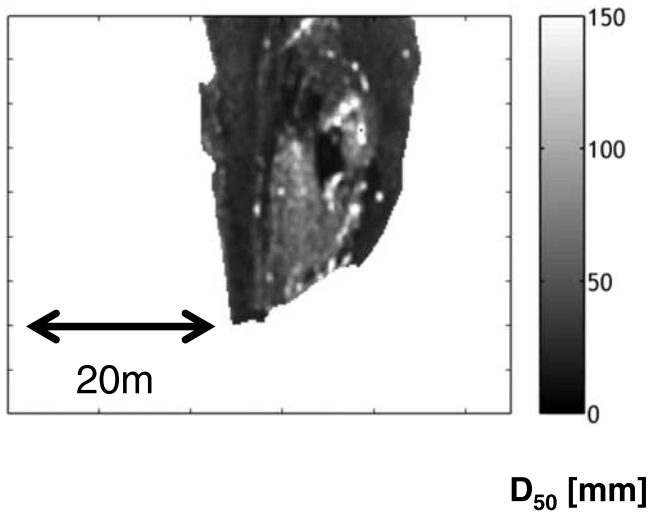

Figure 5. Example of a grain size map calculated with the optimal method, local semivariance, and 33 pixel × 33 pixel (i.e., 99 cm × 99 cm) sampling window, applied to the image in Figure 1a.

consider the possible effects of having particles sizes smaller than pixel ground footprint size. As discussed in section 2, the main source of brightness variations in gravel images is the clast-shadow contact areas whose size scales with the particle size. Therefore, in areas where the image pixel ground footprint is significantly greater than particle size, both clast and shadow contact areas will be contained within any given pixel. This will average out the brightness, and the variation will be lost, which could be expected to lead to a failure of grain size estimation methods for particle sizes smaller than the pixel ground footprint sizes. However, error assessment results for grain size estimates derived from 3 cm imagery using local semivariance calculated over 33 pixels $\times$ 33 pixel sampling windows show that mean error was -0.28 cm with a standard deviation of 1.39 cm. Both these results are well below the pixel size which demonstrates the subpixel sensitivity of the method. However, examination of Figure 4a shows a departure from linearity at small sizes. This loss of quality at small scale can partially be attributed to particle size being smaller than median grain size. Furthermore, a size-dependent noise effect is present. Examination of Figure 4a reveals a series of points near the origin with a grain size of 0 mm (sand) and semivariance values ranging from 5 to 50. Close examination of the photosieving images and the airborne images shows the presence of small woody debris and shrubs. The color of the debris and shrubs is often in contrast to the color of neighboring pixels. Therefore this can have an effect on image texture and semivariance. In the case of coarse clasts, where the pixel size is smaller than the particle size, the texture and semivariance values associated to the clasts themselves are high, and the debris has little effect on the correlation relationship. In the case of clasts smaller than the pixel size, the pixel values represent averaged values of light-dark contact areas. Therefore associated semivariance and texture values are small, and the debris, which is often larger than the pixel size, can significantly increase the total observed texture and semivariance values and therefore cause a size-dependent departure from linear behavior. Hence loss of quality can be expected in areas where the particle size is significantly smaller than the pixel size. The failure of grain size estimation from 10 cm resolution imagery can partially be attributed to pixel size versus particle size effects. In the grain size map shown in Figure 5, only 4% of clasts (by surface) were larger than 10 cm (i.e., 100 mm). However, woody debris and small bushes frequently exceed 10 cm in diameter. Therefore it should be expected that attempts at grain size estimation from 10 cm resolution imagery may fail since most particles are smaller than the pixel size and debris is frequently larger than the pixel size.

5.2. Performance of Texture Versus Performance of Semivariance

[31] After model validation, local image semivariance gives better results then local image texture and was selected as the best method for grain size mapping (Figure 5). Despite the fact that the local image texture model had a comparable quality, image texture failed at the validation stage. The likely explanation for this is that image texture remains sensitive to illumination changes that can occur as a result of changes in daylight or camera exposure times. The images used for model calibration were taken consecutively, while those used for validation, scattered over 10 km, were taken over a greater time span during which lighting conditions could have changed slightly. These changes in illumination could potentially alter the predictive relationship between texture and grain size and cause the failure of the texture model at the validation stage. It is therefore possible that a better illumination correction procedure would improve this situation. Another possible explanation for the failure of the texture method lies in the resampling of the colors in the original image. As stated previously, during the calculation of the cooccurrence matrix, images were resampled to 32 gray levels in order to reduce processing time to manageable levels. This resampling reduces the information content in the image by smoothing small differences in gray levels. Since image semivariance uses brightness differences in the raw 8 bit gray level image, maximum image information is preserved and the semivariance method can be expected to be more sensitive to small changes in color patterns. Therefore semivariance was selected as the method used for gain size estimation.

5.3. Grain Size Data Quality

[32] The quality of the semivariance-based grain size estimations can be quantified from mean error estimates and their standard deviation. The mean error of -1.4% obtained during validation can be interpreted as a bias, and the standard deviation of 15.4% can be interpreted as a precision of $\pm 15.4\%$ for the method. This error is high compared to field methods which can have precisions below $\pm 10\%$ [*Bunte and Abt*, 2001]. However, the automation of the process and the surfaces that can be covered make this error acceptable. Given that the validation data consisted of bulk samples and that the calibration data consisted in photosieving grain size data, a bias was expected during validation. The obtained bias of -1.4% therefore seems to support the findings of *Ibbeken and Schleyer* [1986], who found that the bias associated to photosieving was sufficiently small to neglect correction factors. Furthermore, the small reported bias confirms field observations that clasts in the study river are generally weakly imbricated.

[33] The most likely sources of error affecting the model calibration can be associated to lighting conditions. While the semivariogram is not sensitive to lighting intensity since it operates on absolute differences, it may be sensitive to changes in lighting direction. This may affect the size of clast shadows and can therefore change both image texture and semivariance. For this reason, imagery was not collected in early morning or evening.

5.4. Comparison to Other Methods of Grain Size Estimation From Airborne Images

[34] With an R^2 of 0.96, these results surpass those of *Verdú et al.* [2003]. The most likely explanation for this improved performance is the use of two-dimensional semivariance as opposed to one-dimensional semivariance. Images are by definition two-dimensional. Therefore the use of two-dimensional semivariance makes more efficient use of the information content in the imagery and improves the estimation of the sill value.

5.5. Future Research

[35] The first important aspect requiring further research is the measurement of grain sizes in submerged areas. The

dry bed areas typically represent a small fraction of the total river channel area. The conventional solution to this problem is to fly the airborne survey in periods of low flow. However, this solution still provides a partial view of the riverbed. Therefore a method to measure grain sizes within the wetted perimeter from airborne imagery would be highly useful. Examination of air photos taken in fluvial environments shows that for shallow areas, some texture is visible on the riverbed. It is therefore possible that methods similar to those presented in this article could yield usable estimates of grain sizes for greater areas of the wetted perimeter. The major question that remains is the quality that can be achieved since the presence of a water interface will severely degrade image quality even if turbidity is low. It can therefore be expected that the quality of the grain sizes estimates will be much lesser than those presented here. However, even if of lesser quality, these estimates could still be of use in many fields of research.

[36] Further investigation is also required to assess the universality of the grain size mapping method presented here. This two-dimensional semivariance-based D_{50} mapping method relies on image properties that exist in any image, and therefore it is reasonable to hypothesize that the method is transferable to other river systems. However, several issues need to be investigated. The effect of varying river lithologies on the precision of the method and on the calibration relationship for the empirical model should be studied in order to demonstrate that the method is applicable on any river. Additionally, a better understanding of the effect of the illumination angle during image collection on the model calibration could potentially improve the resulting data quality.

6. Conclusion

[37] It has been demonstrated that reliable grain size estimations of the exposed dry bed areas of a river channel can be obtained from digital airborne imagery, provided that image resolution, sampling window size, and ground truth grain size scale are adjusted with respect to particle size and uniform gravel patch scale following equations (3)–(6). If properly calibrated and adjusted, the methods presented in this study allow for fully automated mapping of grain size with an error of ±15.4% at a spatial resolution of 99 cm. Such methods, combined with appropriate data management, will therefore allow for studies and modeling of processes on a scale which has been difficult to work with in the past.

Notation

D distance separating two image pixels, in pixels.
$\vec{d}$ direction between two image pixels, degrees.
P cooccurrence matrix, dimensionless.
L number of rows and columns in the cooccurrence matrix.
I textural inertia, dimensionless.
γ semivariance, square of the units of the variable of interest.
Z spatial variable of interest used in semivariance calculations, any unit.
(M, N) image dimensions, in pixels.
p lag value in the x direction used in semivariance calculations, in pixels.
q lag values in the y direction used in semivariance calculations, in pixels.
W number of rows and columns in sampling window methods.
D_{50} median grain size, mm.
SS Minimum widow size to achieve a stable semivariance sill plane.
GP Size of a uniform gravel patch, cm.
GT Size of the sampling area for ground truth data, cm.
R Image resolution, cm.

[38] **Acknowledgments.** The authors would like to thank Chad Davey for supplying the unpublished grain size data that were used as validation data. The GEOSALAR project is funded by the GEOIDE networks of centers of excellence. This work receives additional funding from the NATEQ postdoctoral scholarship program. This is a contribution to the program of the Centre Interuniversitaire de Recherche sur le saumon atlantique (CIRSA).

References

Adams, J. (1979), Gravel size analysis from photographs, *J. Hydraul. Div. Am. Soc. Civ. Eng.*, *105*(HY10), 1247–1255.

Baret, F., V. C. Vanderbilt, M. D. Steven, and S. Jacquemoud (1994), Use of spectral analogy to evaluate canopy reflectance sensitivity to leaf optical properties, *Remote Sens. Environ.*, *48*, 253–260.

Bergeron, N. E. (1998), Scale-space analysis of stream-bed roughness in coarse gravel-bed streams, *Math. Geol.*, *28*(5), 537–561.

Borel, C. C., and S. A. W. Gerstl (1994), Nonlinear spectral mixing models for vegetative and soil surfaces, *Remote Sens. Environ.*, *47*, 403–416.

Bray, D. I. (1982), Flow resistance in gravel-bed rivers, in *Gravel-Bed Rivers*, edited by R. D. Hey, J. C. Bathurst, and C. R. Thorne, pp. 109–138, John Wiley, Hoboken, N. J.

Bunte, K., and S. R. Abt (2001), Sampling surface and subsurface particle-size distributions in wadable gravel-and cobble-bed streams for analyses in sediment transport, hydraulics and streambed monitoring, *Gen. Tech. Rep. U. S. Dep. Agric.*, *RMRS-GTR-74*.

Butler, J. B., S. N. Lane, and J. H. Chandler (2001a), Automated extraction of grain-size data from gravel surfaces using digital image processing, *J. Hydraul. Res.*, *39*(5), 1–11.

Butler, J. B., S. N. Lane, and J. H. Chandler (2001b), Characterisation of the structures of river-bed gravels using two-dimensional fractal analysis, *Math. Geol.*, *333*, 301–330.

Carbonneau, P. E., S. N. Lane, and N. E. Bergeron (2003), Cost-effective non-metric close-range digital photogrammetry and its application to a study of coarse gravel river beds, *Int. J. Remote Sens.*, *24*, 2837–2854.

Castleman, K. R. (1996), *Digital Image Processing*, 666 pp., Prentice-Hall, Old Tappan, N. J.

Church, M. A., D. G. Mclean, and J. F. Wolcott (1987), River bed gravels: Sampling and analysis, in *Sediment Transport in Gravel-Bed Rivers*, edited by C. R. Thorne, J. C. Bathurst, and R. D. Hey, John Wiley, Hoboken, N. J.

Clifford, N. J., A. Robert, and K. S. Richards (1992), Estimation of flow resistance in gravel-bed rivers: A physical explanation of the multiplier of roughness length, *Earth Surf. Processes Landforms*, *17*, 529–534.

Conners, R. W., M. M. Trivedi, and C. A. Harlow (1984), Segmentation of a high resolution urban scene using texture operators, *Comput. Vision Graphics Image Processing*, *25*, 273–310.

Cunjak, R. A. (1988), Behaviour and microhabitat of young Atlantic salmon (*Salmo salar*) during winter, *Can. J. Fish. Aquat. Sci.*, *45*, 2156–2160.

Fausch, K. D., C. E. Torgerson, C. V. Baxter, and H. W. Li (2002), Landscapes to riverscapes: Bridging the gap between research and conservation of stream fishes, *BioScience*, *52*(6), 483–498.

Guay, J. C., D. Boisclair, D. Rioux, M. Leclerc, M. Lapointe, and P. Legendre (2000), Development and validation of numerical habitat models for juveniles of Atlantic salmon (*Salmo salar*), *Can J. Fish Aquat. Sci.*, *57*, 2065–2075.

Haralick, R. M. (1979), Statistical and structural approaches to texture, *Proc. IEEE*, *67*(5), 786–804.

Haralick, R. M., K. Shanmugan, and I. Dinstein (1973), Textural features for image classification, *IEEE Trans. Syst. Man Cybern.*, *3*(6), 610–621.

Heggenes, J. (1996), Habitat selection by brown trout (*Salmo trutta*) and young Atlantic salmon (*S. salar*) in streams: Static and dynamic hydraulic modelling, *Reg. Rivers Res. Manage.*, *12*, 155–169.

Hey, R. D., and C. R. Thorne (1983), Accuracy of surface samples from gravel bed material, *J. Hydraul. Eng.*, *109*(6), 842–851.

Ibbeken, H., and R. Schleyer (1986), Photo sieving: A method for grainsize analysis of coarse-grained, unconsolidated bedding surfaces, *Earth Surf. Processes Landforms*, *11*, 59–77.

Institute of Electrical and Electronics Engineers (IEEE) (1990), *IEEE Standard Glossary on Image Processing and Pattern Recognition Terminology, 610. 4*, IEEE Press, Piscataway, N. J.

Legleiter, C. J., W. A. Marcus, and R. L. Lawrence (2002), Effects of sensor resolution on mapping in-stream habitats, *Photogramm. Eng. Remote Sens.*, *68*(8), 801–807.

Middleton, G. V., and J. B. Southard (1984), *Mechanics of Sediment Movement*, *SEPM Short Course*, *3*, 401 pp.

Miranda, F., and J. Carr (1994), Application of the semivariogram textural classifier for vegetation discrimination using SIR-B data of Borneo, *Int. J. Remote Sens.*, *13*, 2349–2354.

Otsu, N. (1979), A threshold selection method from gray-level histograms, *IEEE Trans. Syst. Man Cybern.*, *9*(1), 62–66.

Rice, S., and M. Church (1996), Sampling superficial fluvial gravels: The precision of size distribution percentile estimates, *J. Sediment. Res.*, *66*(3), 654–665.

Rice, S., and M. Church (1998), Grain size along two gravel-bed rivers: Statistical variations, spatial patterns and sedimentary links, *Earth Surf. Processes Landforms*, *23*, 345–363.

Rimmer, D. M., U. Paim, and R. L. Saunders (1983), Changes in the selection of microhabitat by juvenile Atlantic salmon (*Salmo salar*) at the summer-autumn transition in a small river, *Can. J. Fish. Aquat. Sci.*, *41*, 469–475.

Robert, A. (1991), Fractal properties of simulated bed profiles in coarse-grained channels, *Math. Geol.*, *23*(3), 367–382.

Rossi, R. E., D. J. Mulla, A. G. Journel, and E. H. Franz (1992), Geostatistical tools for modeling and interpreting ecological spatial dependence, *Ecol. Monogr.*, *62*, 277–314.

Verdú, J. M., R. J. Batalla, and J. A. Martinex-Cassasnovas (2003), Estimating grain size distributions of a gravel riverbed at reach scale from detailed aerial photos, geostatistics and digital image processing (Isabena River, Spain), paper presented at the Braided Rivers Conference, Br. Geomorphol. Res. Group, London, April.

Whitman, S. M., E. H. Moran, and R. T. Ourso (2003), Photographic techniques for characterizing streambed particle sizes, *Trans. Am. Fish. Soc.*, *132*, 605–610.

Wiberg, P. L., and J. D. Smith (1987), Calculations of the critical shear stress for motion of uniform and heterogeneous sediments, *Water Resour. Res.*, *23*, 1471–1480.

Winterbottom, S. J., and D. J. Gilvear (1997), Quantification of channel bed morphology in gravel-bed rivers using airborne multispectral imagery and aerial photography, *Regul. Rivers*, *13*(6), 489–499.

Wolman, M. G. (1954), A method of sampling coarse bed material, *Eos Trans. AGU*, *35*, 951–956.

Wright, A., W. A. Marcus, and R. Aspinall (2000), Evaluation of multispectral, fine scale digital imagery as a tool for mapping stream morphology, *Geomorphology*, *33*(2), 107–120.

Wulder, M., and B. Boots (1998), Local spatial autocorrelation characteristics of remotely sensed imagery assessed with the Getis statistic, *Int. J. Remote Sens.*, *19*, 2223–2231.

Zhang, Y. (2000), A method for continuous extraction of multispectraly classified urban rivers, *Photogramm. Eng. Remote Sens.*, *66*(8), 991–999.

N. E. Bergeron, Centre Eau, Terre et Environnement, Institut National de la Recherche Scientifique, 2600 boul Laurier, suite 640, Sainte-Foy, Quebec, Canada G1V 4C7.

P. E. Carbonneau and S. N. Lane, Department of Geography, University of Durham, Durham DH1 3HP, UK. (p.carbonneau@geog.leeds.ac.uk)